Journal of Electronic Materials (2022) 51:3359–3363
https://doi.org/10.1007/s11664-022-09633-4

TOPICAL COLLECTION: SYNTHESIS AND ADVANCED CHARACTERIZATION OF MAGNETIC OXIDES

The Inverse and Conventional Magnetocaloric Effects in $Ni_{0.4}Cu_{0.2}Zn_{0.4}Fe_{2-x}Dy_xO_4$ Nanoferrites Over an Extraordinary Temperature Range

Mahmoud A. Hamad[1] · **Hatem R. Alamri**[2]

Received: 2 February 2022 / Accepted: 4 April 2022 / Published online: 7 May 2022

Abstract
The magnetocaloric effect (MCE) of $Ni_{0.4}Cu_{0.2}Zn_{0.4}Fe_{2-x}Dy_xO_4$ (x = 0.02, 0.03, and 0.04) nanoferrites is simulated using a phenomenological model. The analysis indicates that the MCE of $Ni_{0.4}Cu_{0.2}Zn_{0.4}Fe_{2-x}Dy_xO_4$ nanoferrites is strongly influenced by Dy content in both conventional and inverse MCE. For conventional MCE, the full-width at half-maximum (δT_{FWHM}) has significant values, ranging between 200 K and 258 K for $Ni_{0.4}Cu_{0.2}Zn_{0.4}Fe_{2-x}Dy_xO_4$ nanoferrites. However, for inverse MCE, δT_{FWHM} ranges between 25 and 55 K. The MCE of the $Ni_{0.4}Cu_{0.2}Zn_{0.4}Fe_{2-x}Dy_xO_4$ system covers an extensive temperature range and is a particularly interesting prospect for nitrogen and hydrogen liquefaction.

Keywords Phenomenological model · magnetocaloric effect · nanoferrites

Introduction

The magnetocaloric effect (MCE) is a magneto-thermodynamic phenomenon that arises in the absorption or generation of heat by such magnetically ordered material when the applied magnetic field (H_{exe}) is changed.[1–5] Because of the advantages of magnetic refrigeration (MR) including environmental safety, higher efficiency, and the ability to be implemented in a wide range of temperatures, it has become an appealing replacement for traditional refrigeration systems.[6–11] Many decades have been spent studying a broad range of materials that demonstrate acceptable magnetocaloric (MC) characteristics at ambient or even low temperatures.[9,12–18] MR could be used for gas liquefaction, specifically helium, nitrogen, and hydrogen liquefaction, as well as for research activities and low-temperature space applications.[19] MR reflects the concept of applying MCE to MC material at temperatures near that of a magnetic phase transition.[14–19] An initial response of adiabatic demagnetization occurs in traditional MCE as a cooling action in MC material, which is carried out with the abrupt removal of the H_{exe}.[20–24] However, adiabatic magnetization can cool MC materials that experience a sudden increase in the H_{exe}, which is called an inverse MCE.[4] This inverse MCE is seen in antiferromagnetic (AFM) materials over the AFM transition temperature range.

Magnetic nanoparticles (MNPs) are an excellent replacement for bulk MCE materials due to the ease of assembly in the form of thin film and other desirable features, including their influence over the ΔS_M throughout the superparamagnetic–blocking transition.[24] Theoretically, decreasing the particle size to nearer the single magnetic domain enhances ΔS_M by many orders of magnitude when contrasted with ΔS_M in bulk materials.[24] Furthermore, the high surface area of nano-materials would enhance the exchange of heat with the surroundings, and it would be possible to modify the exchange of heat between MNPs and the surroundings by carefully designing core structures. Furthermore, different MNP sizes have the potential to achieve a broader range of cooling.[25,26]

The Ni-Cu-Zn ferrite is a soft ferrite with high T_{MPT}, large electrical resistivity and extreme permeability in the radio-frequency range. Ni-Cu-Zn ferrites are used primarily as

✉ Mahmoud A. Hamad
m_hamad76@yahoo.com

[1] Basic Science Department, Higher Institute of Engineering and Technology, Alexandria, Egypt

[2] Physics Department, Aljamoum University College-Umm Al-Qura University, Makkah 21955, Saudi Arabia

transformer cores, inductors, recording heads, and deflection yokes.[27,28] Optimizing NiCuZn ferrites by modifying the portions of metal ions in the formula or doping with new metals has recently been investigated. When the ferric ion was partially replaced with RE ions (Gd^{3+} Eu^{3+}, Sm^{3+}, and Pr^{3+}), a distortion in the crystal structure of the $Ni_{0.4}Cu_{0.2}Zn_{0.4}$ ferrite was noted, as was an improvement in its magnetic properties.[29]

Almessiere et al. used the sol-gel method to prepare $Ni_{0.4}Cu_{0.2}Zn_{0.4}Fe_{2-x}Dy_xO_4$ ($x \leq 0.04$) nanoferrites, which showed superparamagnetic behaviour and broadly second-order FM–paramagnetic phase transitions for all samples, along with an AFM–paramagnetic phase transition at extremely low temperatures.[30] We were thus highly motivated to investigate the MCE of $Ni_{0.4}Cu_{0.2}Zn_{0.4}Fe_{2-x}Dy_xO_4$ nanoferrites in this work, based on this useful point. In this research, a phenomenological model (PM) is used to investigate the thermomagnetic properties of $Ni_{0.4}Cu_{0.2}Zn_{0.4}Fe_{2-x}Dy_xO_4$ nanoferrites using simulated magnetization temperature curves, resulting in ΔS_M, heat capacity change ($\Delta C_{P,H}$), and relative cooling power (RCP).

Theoretical Considerations

The PM provides the relationship between magnetization (M) and temperature (T) as follows[31,32]:

$$M(T) = \left(\frac{M_i - M_f}{2}\right)\left[\tanh(\alpha(T_{MFT} - T))\right] + \beta(T - T_{\mathrm{MFT}}) + \left(\frac{M_i + M_f}{2}\right) \quad (1)$$

where M_i is an initial value of magnetization at the FM–paramagnetic or AFM–paramagnetic transition, and M_f is a final value of this transition as shown in Fig. 1, where $\alpha = \frac{2(\beta-\gamma)}{M_i - M_f}$., $\beta = \left(\frac{dM}{dT}\right)_{average}$ for FM or AFM phase, and $\gamma = \left(\frac{dM}{dT}\right)_{T=T_{MFT}}$.

Results and Discussion

To simulate the MCE of $Ni_{0.4}Cu_{0.2}Zn_{0.4}Fe_{2-x}Dy_xO_4$, PM parameters for $Ni_{0.4}Cu_{0.2}Zn_{0.4}Fe_{2-x}Dy_xO_4$ were obtained directly from experimental results (magnetization vs temperature), as described in Almessiere et al.[30] The magnetization versus temperature for $Ni_{0.4}Cu_{0.2}Zn_{0.4}Fe_{2-x}Dy_xO_4$ nanoferrites measured at 0.01T is depicted in Fig. 2, with experimental data from Almessiere [30] expressed by symbols and simulated data expressed by dashed lines.

There appears to be reasonable agreement between the experimental and theoretical values of M(T) for $Ni_{0.4}Cu_{0.2}Zn_{0.4}Fe_{2-x}Dy_xO_4$ nanoferrites, implying that PM is an appropriate model for fitting FM–paramagnetic and AFM

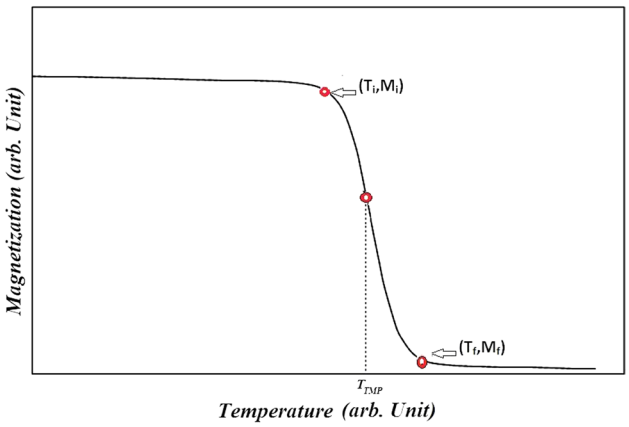

Fig. 1 The dependence of isofield magnetization vs temperature.

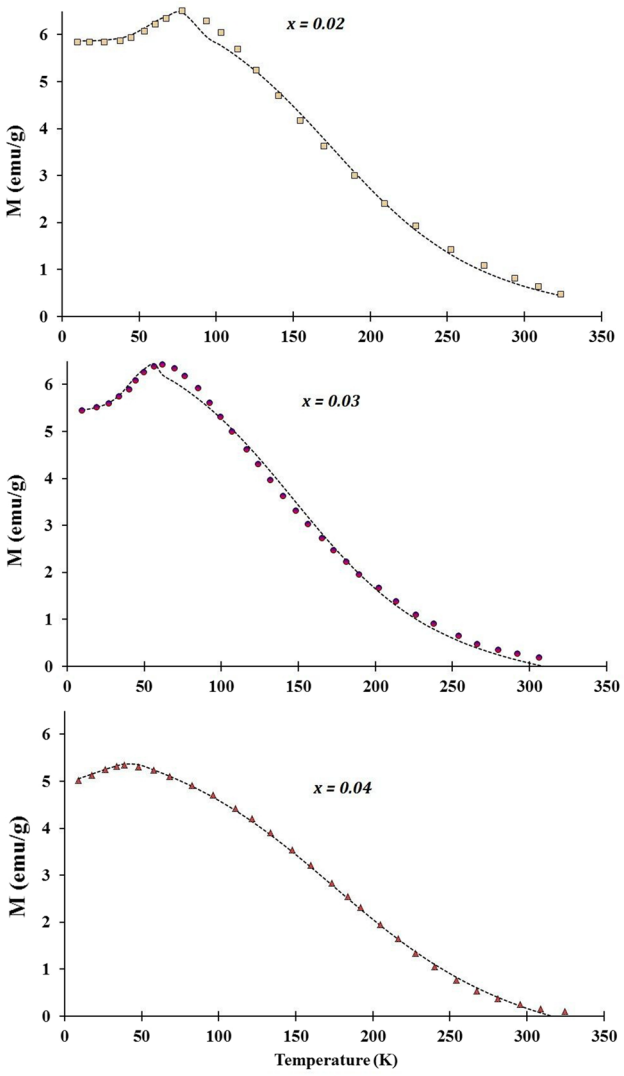

Fig. 2 Magnetization vs temperature for $Ni_{0.4}Cu_{0.2}Zn_{0.4}Fe_{2-x}Dy_xO_4$ nanoferrites in H_{exe} of 0.01 T. The dashed curves are modelled results and symbols represent experimental data from Ref. 30.

transitions. Interestingly, it seems that, in addition to conventional MCE, an inverse MCE for $Ni_{0.4}Cu_{0.2}Zn_{0.4}Fe_{2-x}Dy_xO_4$ nanoferrites is present at very low temperatures, as we will later explore.

ΔS_M of $Ni_{0.4}Cu_{0.2}Zn_{0.4}Fe_{2-x}Dy_xO_4$ nanoferrites under an adiabatic magnetic field shift (ΔH) of 0.01 T is formulated by

$$\Delta S_M(T,\Delta H) = -0.01 \times \left(\alpha \times \left(\frac{M_i - M_f}{2}\right) \times \operatorname{sech}^2(\alpha \times (T_{MPT} - T)) + \beta\right). \quad (2)$$

The maximum ΔS_M (ΔS_{Max}) can be determined as follows:

$$\Delta S_{Max} = -0.01 \times \left(\alpha \times \left(\frac{M_i - M_f}{2}\right) + \beta\right) \quad (3)$$

The simulated temperature dependence of ΔS_{M} for $Ni_{0.4}Cu_{0.2}Zn_{0.4}Fe_{2-x}Dy_xO_4$ nanoferrites is depicted in Fig. 3. Importantly, the thermomagnetic behaviour of $Ni_{0.4}Cu_{0.2}Zn_{0.4}Fe_{2-x}Dy_xO_4$ nanoferrites is strongly dependent on Dy content, leading to the conclusion that the thermomagnetic behaviour of $Ni_{0.4}Cu_{0.2}Zn_{0.4}Fe_{2-x}Dy_xO_4$ nanoferrites is characterized as a conventional MCE over temperatures higher than 78, 62, and 39 K for doping levels $x = 0.02$, 0.03, and 0.04, respectively. However, the thermomagnetic behaviour of $Ni_{0.4}Cu_{0.2}Zn_{0.4}Fe_{2-x}Dy_xO_4$ nanoferrites is characterized as an inverse MCE at lower temperatures. As a result, $Ni_{0.4}Cu_{0.2}Zn_{0.4}Fe_{2-x}Dy_xO_4$ nanoferrites could be operated in MR that uses magnetization and demagnetization processes to exploit both positive and negative magnetic entropy variations. $|\Delta S_{\mathrm{Max}}|$ is significantly reduced when the Dy content is high. The fact that Dy^{+3} ions are favoured to exist in the B sites, which can be attributed to their large ionic radii, could explain this decreasing trend. As a result of the Fe^{3+} replacement by Dy^{3+}, the crystal symmetry is reduced, implying that the distance between Dy–O will be smaller than the distance between Fe–O.[33] Consequently, some of the corresponding ions display aligned antiparallel moments with regard to others in these sites, causing a drop in net magnetic moments just on B sites. As Dy^{3+} content increases, further cations on B sites exhibit antiparallel moments. To put it another way, the decrease in $|\Delta S_{\mathrm{M}}|$ at high content in samples is due to surface spin effects and cation distribution on various sites. Despite the fact that magnetic moments are no longer directed linearly, nonlinear spins of magnetic ions exist due to spin frustration.[33] The increase in migration of Fe^{3+} cations from tetrahedral to octahedral sites with the goal of occupying the increasing Dy^{3+} ions causes the reduction drop in the $|\Delta S_{\mathrm{M}}|$. The increased presence of Fe^{3+} cations in octahedral B sites due to site preference causes an increase in spin canting and antiparallel spin coupling, reducing the $|\Delta S_{\mathrm{M}}|$ and weak super-exchange interactions between tetrahedral and octahedral sites, lowering the magnetization.[34] Furthermore, the ionic radii for various elements, and also the critical A–B super-exchange interactions between many magnetic ions, could be used to deduce the influence of Dy^{3+} ions on magnetic characteristics. Dy^{3+} ions have an ionic radius of 0.912 Å, indicating that they prefer to be found on B sites. The ionic radii that are subjected to substitution differ greatly, causing disorder in the electronic states and internal strains in the crystal structure. This has an impact on the A–B super-exchange interactions between metal sites A and B.[35,36] Furthermore, variations in the drop in $|\Delta S_{\mathrm{M}}|$ at high Dy^{3+} content can be explained by crystallite size variation. Indeed, as the Dy^{3+} content increases, the crystallite size decreases, resulting in a reduction in magnetization and, as a result, a decrease in $|\Delta S_{\mathrm{M}}|$.

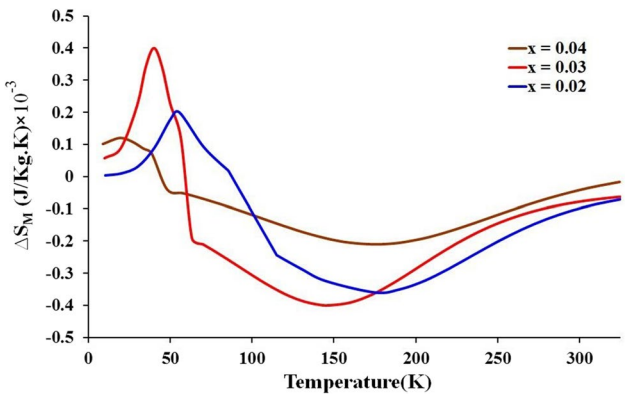

Fig. 3 ΔS_{M} vs temperature for $Ni_{0.4}Cu_{0.2}Zn_{0.4}Fe_{2-x}Dy_xO_4$ nanoferrites in ΔH of 0.01 T.

The $|\Delta S_{\mathrm{Max}}|$ and full-width at half-maximum (δT_{FWHM}) of the S_{M} curve are used to account for RCP as follows.

$$\mathrm{RCP} = \left|\Delta S(T, H_{\max})\right|_{\mathrm{Max}} \times \delta T_{\mathrm{FWHM}}, \quad (4)$$

where δT_{FWHM} can be obtained as follows:

$$\delta T_{\mathrm{FWHM}} = \frac{2}{\alpha} \times \cosh^{-1}\left(\sqrt{\frac{2(M_i - M_f) \times \alpha}{(M_i - M_f) \times \alpha + 2\beta}}\right). \quad (5)$$

For conventional MCE, the calculations show that δT_{FWHM} has significant values, ranging between 200 K and 258 K for $Ni_{0.4}Cu_{0.2}Zn_{0.4}Fe_{2-x}Dy_xO_4$ nanoferrites under ΔH of 0.01 T. However, for inverse MCE, the range of δT_{FWHM} is between 25 K and 55 K. Furthermore, for conventional MCE, RCP is between 0.05 J/Kg and 0.08 J/Kg,

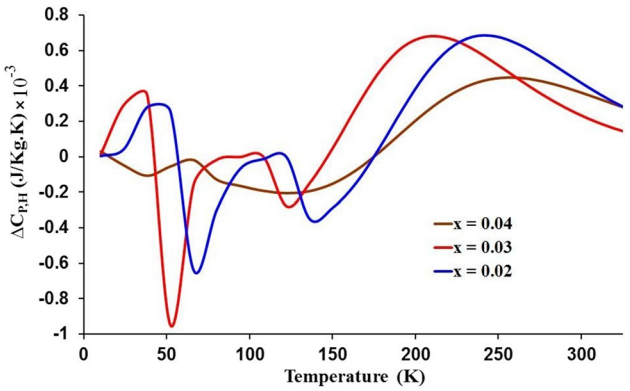

Fig. 4 $\Delta C_{P,H}$ vs temperature for $Ni_{0.4}Cu_{0.2}Zn_{0.4}Fe_{2-x}Dy_xO_4$ nanoferrites in ΔH of 0.01T.

whereas for inverse MCE, RCP is between 0.007 J/Kg and 0.01 J/Kg.

The characterization of curves for $Ni_{0.4}Cu_{0.2}Zn_{0.4}Fe_{2-x}Dy_xO_4$ nanoferrites can be explained as follows, according to the PM model[31,32]:

$$\Delta C_{P,H} = -0.01\alpha^2 \times T \times (M_i - M_f) \times \tanh(\alpha \times (T_{MPT} - T)) \operatorname{sech}^2(\alpha \times (T_{MPT} - T)). \quad (6)$$

$\Delta C_{P,H}$ versus temperature simulations for $Ni_{0.4}Cu_{0.2}Zn_{0.4}Fe_{2-x}Dy_xO_4$ nanoferrites at ΔH of 0.01 T are shown in Fig. 4. Over the range of the AFM transition, the simulated $\Delta C_{P,H}$ of all samples varies from a positive to a negative value. However, over the range of the FM transition, an inverse characterization is observed. Finally, $Ni_{0.4}Cu_{0.2}Zn_{0.4}Fe_{2-x}Dy_xO_4$ nanoferrites are fascinating MC materials in MR, particularly between 10 and 325 K. Furthermore, they have high resistivity, small hysteresis, low loss of eddy current, and the energy loss is negligible.[30] The MCE and the electrocaloric effect both contribute to the future of refrigeration technology.[37–67]

Conclusion

MCE simulations were performed on $Ni_{0.4}Cu_{0.2}Zn_{0.4}Fe_{2-x}Dy_xO_4$ nanoferrites synthesized using the sol–gel method. The simulation results show that this PM is an efficient model for calculating the thermomagnetic properties of $Ni_{0.4}Cu_{0.2}Zn_{0.4}Fe_{2-x}Dy_xO_4$ nanoferrites for both FM–AFM and FM–paramagnetic transitions. The thermomagnetic behaviour of $Ni_{0.4}Cu_{0.2}Zn_{0.4}Fe_{2-x}Dy_xO_4$ nanoferrites demonstrates both conventional and inverse MCE. The $Ni_{0.4}Cu_{0.2}Zn_{0.4}Fe_{2-x}Dy_xO_4$ nanoferrites are an interesting possibility for MR because they cover a wide temperature range, especially liquefaction of nitrogen and hydrogen, even at room temperature.

Funding Open access funding provided by The Science, Technology & Innovation Funding Authority (STDF) in cooperation with The Egyptian Knowledge Bank (EKB).

Conflict of interest The authors declare that they have no conflict of interest.

References

1. M. Hsini, S. Hcini and S. Zemni, *J. Supercond. Nov. Magn.* 31, 81 (2018).
2. E.M. Ahmed, O.M. Hemeda, H.R. Alamri and S.M. Elghnam, *Phase Trans.* 94, 835–841 (2021).
3. E.M. Ahmed, H.R. Alamri, S.M. Elghnam, O. Eldarawi, T.E. Tawfik, A.M. Mahmoud, S.E. Elwan, O.M. Hemeda, M.A. Hamad and G.A. Hussein, *Phys Solid State* (2021). https://doi.org/10.1134/S1063783421100024.
4. E.M. Ahmed, O.M. Hemeda, H.R. Alamri, S.M. Elghnam and M.A. Hamad, *Phys. Met. Metallogr.* 122, 1454–1457 (2021).
5. B. Alzahrani, M. Hsini, S. Hcini, M. Boudard, A. Dhahri and M.L. Bouazizi, *J. Low Temp. Phys.* 200, 26–39 (2020).
6. A.M. Ewas, *Ceram. Int.* 43, 7660 (2017).
7. R. Kumar, *Mater. Today* 4, 5544 (2017).
8. A.H. El-Sayed, *J. Supercond. Nov. Magn.* 32, 1447 (2019).
9. M.A. Hamad, *Process. Appl. Ceram.* 9, 11 (2015).
10. N. Mechi, B. Alzahrani, S. Hcini, M.L. Bouazizi and A. Dhahri, *Phase Trans.* 91, 559 (2018).
11. H.R. Alamri, S.M. Elghnam, O.M. Hemeda and M.A. Hamad, *Phys. Solid State* 63, 1332–1336 (2021).
12. E. Villa, C. Tomasi, A. Nespoli, F. Passaretti, G. Lamura and F. Canepa, *J. Mater. Res. Technol.* 9, 2259 (2020).
13. H. Xiang, Y. Xing, F. Dai, H. Wang, L. Su, L. Miao and L. Sheng-Guo, *J. Adv. Ceram.* 10, 385–441 (2021).
14. M. Jeddi, H. Gharsallah, M. Bekri, E. Dhahri and E.E.K. Hlil, *J. Low Temp. Phys.* 198, 135 (2020).
15. A.H. El-Sayed, O.M. Hemeda, M.A. Hamad and A.M. Mohamed, *Eur. Phys. J. Plus.* 134, 227 (2019).
16. A.H. El-Sayed, O.M. Hemeda, M.A. Hamad and A.M. Mohamed, *J. Supercond. Nov. Magn.* 33, 769–773 (2020).
17. M.A. Hamad, O.M. Hemeda, H.M. Alamri, A.M. Mohamed, *J. Supercond. Nov. Magn.* 33, 3853–3856 (2020)
18. A.H. El-Sayed and M.A. Hamad, *Phase Trans.* 92, 517 (2019).
19. M.A. Hamad, H.R. Alamri and M.E. Harb, *J. Low Temp. Phys.* 204, 57–63 (2021).
20. A.H. El-Sayed and M.A. Hamad, *J. Supercond. Nov. Magn.* 31, 4167–4171 (2018).
21. A.H. El-Sayed and M.A. Hamad, *J. Supercond. Nov. Magn.* 31, 1895 (2018).

22. A.H. El-Sayed and M.A. Hamad, *J. Supercond. Nov. Magn.* 31, 4091–4094 (2018).
23. M.A. Hamad, O.M. Hemeda, H.R. Alamri and A.M. Mohamed, *J. Low Temp. Phys.* 202, 121–127 (2021).
24. R.D. McMichael, R.D. Shull, L.J. Swartzendruber, L.H. Bennett and R.E. Watson, *J. Magn. Magn. Mater.* 111, 29 (1992).
25. R.D. Shull, *IEEE Trans. Magn.* 29, 2614 (1993).
26. J. Chen, H. Su, Y. Jing, Y. Li, X. Tang and Q. Lu, *Ceram. Int.* 47, 20638–20642 (2021).
27. B.R. Shaikh, B.G. Toksha, S.E. Shirsath, A. Chatterjee, S. Tonde and S.Q. Chishty, *J. Magn. Magn. Mater.* 537, 168229 (2021).
28. X. Wu, J. Xu, X. Huo, J. Chen, Q. Zhang, F. Huang and L. Li, *J. Eur. Ceram. Soc.* 41, 5193–5200 (2021).
29. H. Harzali, A. Marzouki, F. Saida, A. Megriche and A. Mgaidi, *J. Magn. Magn. Mater.* 460, 89–94 (2018).
30. M.A. Almessiere, Y. Slimani, H. Güngünes, A. Demir Korkmaz, S.V. Trukhanov, S. Guner, F. Alahmari, A.V. Trukhanov and A. Baykal, *Mater. Sci. Eng. B* 270, 115202 (2021).
31. M.A. Hamad, *Phase Trans.* 85, 106 (2012).
32. M.A. Hamad, *Int. J. Thermophys.* 36, 2748 (2015).
33. K. Kamala Bharathi, J. Arout Chelvane and G. Markandeyulu, *J. Magn. Magn. Mater.* 321, 3677–3680 (2009).
34. M.S.R. Prasad, B.B.V.S.V. Prasad, B. Rajesh, K.H. Rao and K.V. Ramesh, *J. Magn. Magn. Mater.* 323, 2115 (2011).
35. P. Samoila, L. Sacarescu, A.I. Borhan, D. Timpu, M. Grigoras, N. Lupu, M. Zaltariov and V. Harabagiu, *J. Magn. Magn. Mater.* 378, 92–97 (2015).
36. A. Sadaqat, M. Almessiere, Y. Slimani, S. Guner, M. Sertkol, H. Albetran, A. Baykal, S.E. Shirsath, B. Ozcelik and I. Ercan, Ceram. *Int.* 45, 22538–22546 (2019).
37. M.A. Hamad and H.R. Alamri, *J. Low Temp. Phys.* 207, 181–189 (2022).
38. M.A. Hamad, *J. Adv. Dielect.* 4, 1450026 (2014).
39. M.A. Hamad, *J. Supercond. Nov. Magn.* 28, 2525–2528 (2015).
40. M.A. Hamad, *J. Supercond. Nov. Magn.* 28, 3365 (2015).
41. M.A. Hamad, *J. Supercond. Nov. Magn.* 29, 2867–2871 (2016).
42. M.A. Hamad, *Int. J. Thermophys.* 34, 1158–1165 (2013).
43. M.A. Hamad, *J. Supercond. Nov. Magn.* 28, 3329–3333 (2015).
44. M.A. Hamad, *J. Adv. Dielect.* 3, 1350008 (2013).
45. M.A. Hamad, O.M. Hemeda, H.R. Alamri, M.E. Harb and A.M. Mohamed, *Phys. Solid State* 63, 709–713 (2021).
46. M.A. Hamad, *J. Supercond. Nov. Magn.* 27, 2569 (2014).
47. M.A. Hamad, *J. Supercond. Nov. Magn.* 29, 539–1543 (2016).
48. M.A. Hamad and H.R. Alamri, *J. Mater. Res. Technol.* 17, 2670–2674 (2022).
49. A.H. El-Sayed and M.A. Hamad, *J. Supercond. Nov. Magn.* 31, 3357 (2018).
50. M.A. Hamad and H.R. Alamri, *J. Supercond. Nov. Magn.* 35, 515–518 (2022).
51. E.M. Ahmed, O.M. Hemeda, H.R. Alamri et al., Magnetocaloric Effect in α'-MnB Nanoparticles. *Russ. J. Phys. Chem.* 96, S101–S104 (2022).
52. M.A. Hamad, *J. Supercond. Nov. Magn.* 31, 337 (2018).
53. M.A. Hamad, *J. Supercond. Nov. Magn.* 27, 223 (2014).
54. M.A. Hamad, *Process. Appl. Ceram.* 11, 225–229 (2017).
55. M.A. Hamad, O.M. Hemeda, H.R. Alamri and A.M. Mohamed, *J. Mater. Res. Technol.* 11, 1356–1361 (2021).
56. M.A. Hamad, *J. Comput. Electron.* 11, 344 (2012).
57. M.A. Hamad, *J. Adv. Dielect.* 3, 1350029 (2013).
58. M.A. Hamad, *J. Supercond. Nov. Magn.* 27, 1777 (2014).
59. M.A. Hamad, O.M. Hemeda, H.R. Alamri and A.M. Mohamed, *Phys. Lett. A.* 394, 127204 (2021).
60. M.A. Hamad, *J. Supercond. Nov. Magn.* 27, 269–272 (2014).
61. M.A. Hamad, *Process. Appl. Ceram.* 10, 33 (2016).
62. M.A. Hamad and H.R. Alamri, *Front. Mater.* 9, 832703 (2022).
63. M.A. Hamad, O.M. Hemeda and A.M. Mohamed, *J. Supercond. Nov. Magn.* 33, 2753–2757 (2020).
64. M.A. Hamad and H.R. Alamri, *Phys. Metals Metallogr.* 122, 1458–1462 (2021).
65. M.A. Hamad, *J. Supercond. Nov. Magn.* 28, 2223 (2015).
66. M.A. Hamad, O.M. Hemeda and A.M. Mohamed, *J. Supercond. Nov. Magn.* 33, 2521–2525 (2020).
67. M.A. Hamad, *J. Supercond. Nov. Magn.* 29, 1539 (2016).